Science of the Total Environment 650 (2019) 515–529

Contents lists available at ScienceDirect

Science of the Total Environment

journal homepage: www.elsevier.com/locate/scitotenv

Normalizing land surface temperature for environmental parameters in mountainous and urban areas of a cold semi-arid climate

Qihao Weng [a,b,c], Mohammad Karimi Firozjaei [d], Majid Kiavarz [d,*], Seyed Kazem Alavipanah [d], Saeid Hamzeh [d]

[a] School of Geography, South China Normal University, Guangzhou, Guangdong 510631, China
[b] College of the Environment & Ecology, Xiamen University, South Xiangan Road, Xiangan District, Xiamen, Fujian 361102, China
[c] Center for Urban and Environmental Change, Department of Earth and Environmental Systems, Indiana State University, Terre Haute, IN 47809, USA
[d] Department of Remote Sensing and GIS, University of Tehran, Tehran, Iran

HIGHLIGHTS

- Normalization of LST relative to environmental parameters is significant in climate.
- Triple-EB model f\or modeling LST increased the accuracy over the Dual-EB model.
- Local optimization was more efficient than regional optimization to normalize LST.
- The developed protocol was applicable both to mountainous and urban areas.

GRAPHICAL ABSTRACT

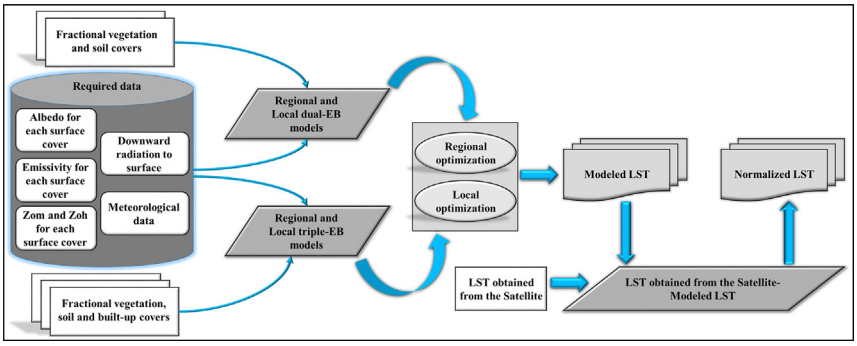

ARTICLE INFO

Article history:
Received 6 June 2018
Received in revised form 12 August 2018
Accepted 3 September 2018
Available online 5 September 2018

Editor: G. Ashantha Goonetilleke

Keywords:
Land surface temperature
Normalization
Environmental parameters
Surface energy balance
Local and regional optimization
Mountain-urban areas

ABSTRACT

Normalization of land surface temperature (LST) relative to environmental factors is of great importance in many scientific studies and applications. The purpose of this study was to develop physical models based on energy balance equations for normalization of satellite derived LST relative to environmental parameters. For this purpose, a set of remote sensing imagery, meteorological and climatic data recorded in synoptic stations, and soil temperatures measured by data loggers were used. For modeling and normalization of LST, a dual-source energy balance model (dual-EB), taking into account two fractions of vegetation and soil, and a triple -source energy balance model (triple-EB), taking into account three fractions of vegetation, soil and built-up land, were proposed with either regional or local optimization strategies. To evaluate and compare the accuracy of different modeling results, correlation coefficients and root mean square difference (RMSE) were computed between modeled LST and LST obtained from satellite imagery, as well as between modeled LST and soil temperature measured by data loggers. Further, the variance of normalized LST values was calculated and analyzed. The results suggested that the use of local optimization strategy increased the accuracy of the normalization of LST, compared to the regional optimization strategy. In addition, no matter the regional or local optimization strategy was employed, the triple-EB model out-performed consistently the dual-EB model for LST normalization. The results show the efficiency of the local triple-EB model to normalize LST relative to environmental parameters. The correlation coefficients were close to zero between all of the environmental parameters and the normalized

* Corresponding author.
E-mail addresses: qweng@indstate.edu (Q. Weng), mohammad.karimi.f@ut.ac.ir (M.K. Firozjaei), kiavarzmajid@ut.ac.ir (M. Kiavarz), salavipa@ut.ac.ir (S.K. Alavipanah), saeid.hamzeh@ut.ac.ir (S. Hamzeh).

https://doi.org/10.1016/j.scitotenv.2018.09.027
0048-9697/

LST. In other words, normalized LST was completely independent of the environmental parameters considered by this research.

1. Introduction

Land surface temperature (LST) is a very important biophysical variable as it reflects the amount of radiation emitted from the surface and sub-surface of the earth, and the exchange of energy between the earth surface and atmosphere. In recent studies, it has been possible to calculate the LST for large areas by using thermal infrared data obtained from thermal remote sensing images and by using physical and quantitative models. LST obtained from thermal remote sensing have been used in numerous studies, including ground and underground thermal sources (Jia et al., 2017; Mansor et al., 1994), environmental monitoring (Wan et al., 2004), energy balance (Friedl, 2002; Weng et al., 2014), geological structure (Ma et al., 2010), climate change and urban phenomena (Okalebo et al., 2016; Voogt & Oke, 2003; Berger et al., 2017; Weng et al., 2004; Firozjaei et al., 2018; Panah et al., 2017), evapotranspiration, soil moisture and water resources management (Jia et al., 2017; Harris et al., 2017; Lievens et al., 2017), and identification of various objects/phenomena (Bellaoui et al., 2017; Eckmann et al., 2008).

The set of environmental parameters, such as temporal and geographical settings, inherent thermal characteristics, biophysical properties, climatic parameters and sub-surface conditions, can cause the heterogeneous spatial and temporal distribution of LST. Normalization of LST relative to environmental parameters is of great importance in many scientific studies and accurate management decisions such as identifying geothermal resources, monitoring the trend of changes in the faults and volcanoes activities, the trend of thermal anomalies and their relationship with earthquake and management and planning of energy consumption in urban environment (Coolbaugh et al., 2007; Gutiérrez et al., 2012; Malbéteau et al., 2017; Mattar et al., 2014). For the earth surface under different conditions, energy balance components include net radiation flux and geothermal sources flux as heaters factors, and soil heat fluxes, sensible heat flux and latent heat flux as surface cooling agents. The energy balance is directly related to the surface environmental parameters. The ultimate goal for normalizing LST relative to environmental parameters is to eliminate and modulate the effect of the net radiation flux, sensible heat flux, and latent heat flux.

Dozier and Outcalt (1979) used the energy balance equations to simulate LST in mountainous regions. In their model, the set of incoming radiation to the surface, albedo, surface roughness, wind speed, relative air humidity, air pressure, and vapor pressure in the air were considered. However, this model did not show effective for heterogeneous areas in terms of vegetation and surface moisture, and was suitable only for dry areas. In their study, direct and diffuse radiations reflected by nearby terrains were not considered for modeling of incoming radiation to the surface. Further, for modeling the environmental lapse rate (ELR), a standard value of 6.5 °C per km was used (Dozier & Outcalt, 1979). Rigon et al. (2006) used the GEotop model for modeling incoming radiation on the surface and its impact on LST. In the model, wind speed and air temperature for the whole region, direct incoming radiation for each pixel were considered according to the local incidence angle, diffuse radiation according to the atmospheric and cloudy transmissivity coefficient, shadow and radiations reflected by nearby terrains effects (Rigon et al., 2006). Jain et al. (2008) investigated the impact of ELR effect on LST in the Satluj River basin. In the study, MODIS and NOAA-AVHRR data were used. The surface area of the study was completely covered by snow. Therefore, surface emissivity coefficient was fixed with spatial variations. The results indicated an inverse linear relationship between LST and elevation parameters. The correlation between LST and elevation parameters for MODIS images showed a stronger correlation than that for AVHRR images, which was caused by the finer spatial resolution of MODIS compared to AVHRR. The correlation varied in different months of the year (Jain et al., 2008). Chen et al. (2009) reviewed the annual LST changes using the normal annual variation field (NAVF) model, and used solar incoming radiation, albedo, geographical location, and topographic conditions to model LST with this model. The relationship between LST and latitude in a specific longitude, in two independent states of elevation, showed very different results (Chen et al., 2009). In the case of altitude dependence, the relationship between LST and latitude along a particular longitude was very weak, but with the elevation independent of this relationship, the correlation coefficient can reach 0.97 (Chen et al., 2009). The results of the study indicated a strong relationship between LST and geographic location and high impact of elevation on LST (Chen et al., 2009). Peters et al. (2012) used the feature space between LST and the vegetation index (VI) to assess evapotranspiration. The results suggested that LST should be normalized to the elevation conditions of the study area in order to use the LST-VI feature space model to investigate evapotranspiration in heterogeneous topographic regions. In a study by Peters et al. (2012), a classified linear regression model was used to investigate the relationship between LST and elevation (Peters et al., 2012). Coolbaugh et al. (2007) used night and day thermal images to identify surface anomalies. In their study, LST obtained from thermal images was normalized relative to the effects of topography, albedo, emissivity and thermal inertia. The energy balance equation was used to normalize LST relative to different environmental parameters, regardless of sensible and latent thermal flux components. Therefore, the proposed model was ineffective for regions with variable biophysical properties (Coolbaugh et al., 2007). Malbéteau et al. (2017) proposed three models of soil and vegetation energy balance equations, multi-linear regression and slope of dry edges for normalization of LST relative to the elevation and illumination effects. In the energy balance model for normalization of LST, sensible and latent heat flux were considered, which was commonly ignored in previous studies due to the complexity of the model. The results of this study indicated that the energy balance equation model performed better than multi-linear regression and slope of dry edges models. In this study, to determine the unknown parameters of the various models, the ordinary least squares (OLS) and regional optimization were used. Moreover, the energy balance equation model for normalizing the LST proposed in the study considered only two fraction covers of vegetation and soil; and it was not suitable for regions with three fraction covers of vegetation, soil and built-up lands (Malbéteau et al., 2017).

The main objective of this study is to develop physical models based on energy balance equations for normalization of LST relative to environmental parameters, including solar radiation, topographic conditions, ELR effect, and surface biophysical characteristics such as albedo, greenness and wetness. The distinction between this study and the previous studies in the context of normalization of LST obtained from satellite images lies in three areas: (1) A physical model based on energy balance equations was presented for three fractions of vegetation, soil and built-up land covers; (2) For solving the unknown parameters in the normalization model, the local optimization strategy was proposed and calculated at the pixel scale; and (3) To solve the unknown parameters related to the LST normalization model in relation to the environmental parameters, the Partial least-squares (PLS) method was used.

2. Materials and methods

2.1. Study area

For implementation and evaluation of the models presented in this study, a mountainous region with an area of 11.09 km^2 was selected. This area is located at the latitude of 35° 48′ 45″, 35° 51′ 00″ north and longitude of 51° 26′ 30″, 51° 28′ 30″ east of World Geodetic System 1984 (WGS 84) located along the Alborz mountain range, north of Tehran city, Iran. This area is located in a semi-arid climate. The weather is cold in winter, and in summer it is warm and dry. During a 45-year period, the highest air temperature in this area was 43° and the lowest temperature was recorded at −15 °C. Rainfall is low and measured at 264.8 mm per year. The average relative humidity is 36%. The average wind speed is 4.5 m per second. The climatic conditions of the area are affected by the mountains in the north and the plain in the south.

Due to the geographical location, the studied area has heterogeneous topographic conditions. Despite of a small area, the elevation varies from 1586 to 3014 m, the slope from 0 to 54.2°, and the aspect from 0 to 359.7°. The heterogeneous distribution of environmental parameters values in this range causes the spatial distribution of LST to be heterogeneous. This area includes all three fractions of vegetation, soil, and built-up land. The geographical location of the studied area, the meteorological station and the soil temperature recording data loggers are shown in Fig. 1.

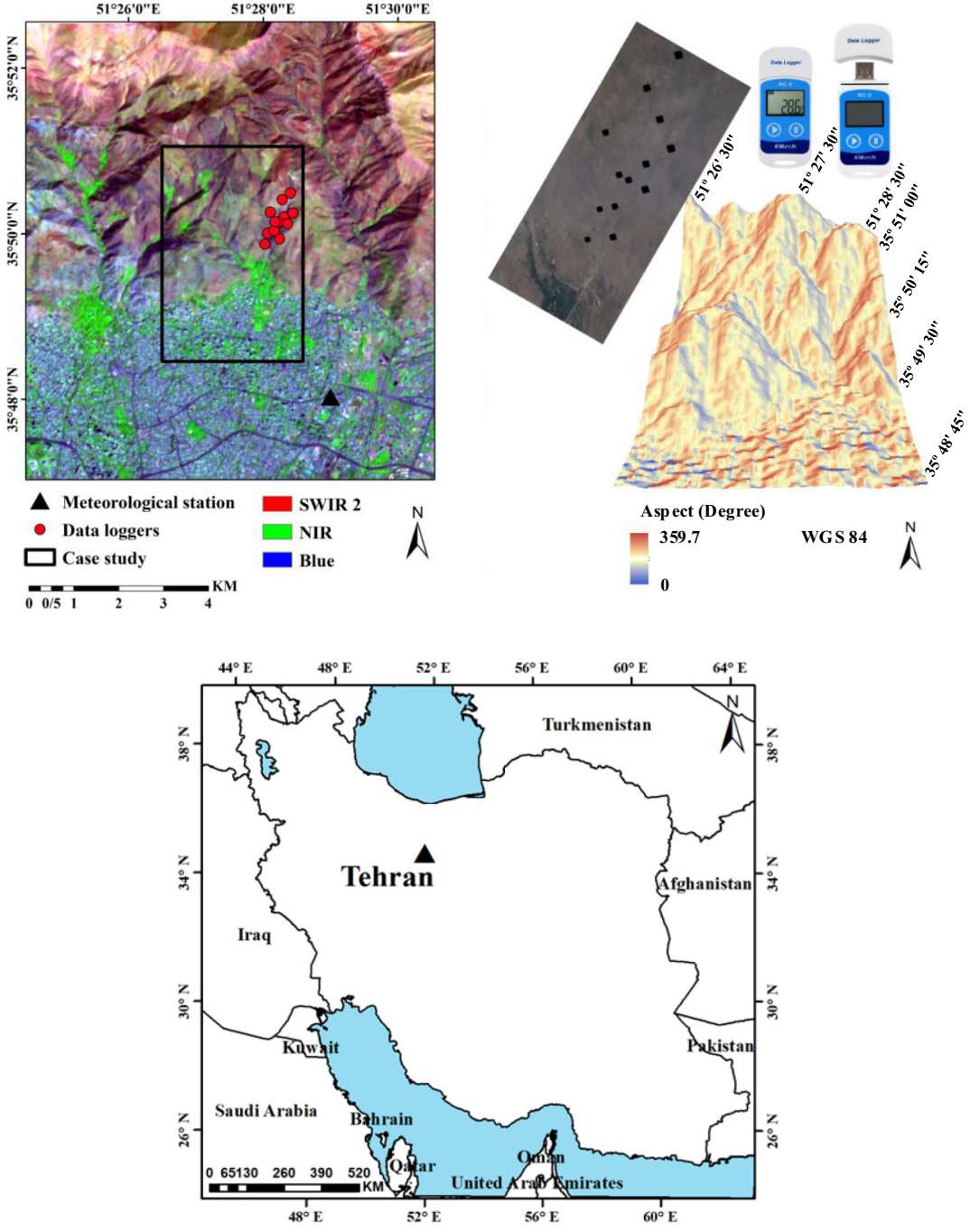

Fig. 1. The geographical location of the study area, the meteorological station and the soil temperature recording data loggers.

2.2. Data

This study used a series of remote sensing, meteorological, climatic and land data sets to implement different models for modeling and normalizing LST. Landsat 8 (Path: 165, Row: 035) image and the MOD07 water vapor product with a spatial resolution of 5000 m of 30 Jun 2017, 17 August 2017 and 02 September 2017, were used. The characteristics of the Landsat 8 bands are shown in Table S1. The Landsat 8 band 10 and 11 thermal data (100 m) were resampled to 30 m. Also, the ASTER Digital Elevation Model (GDEM) of the study region with a spatial resolution of 30 m was used for modeling environmental parameters such as incoming radiation on the surface and ELR effect. In order to assess accuracy of the fractional cover maps obtained from Landsat image 8, a WorldView 2 satellite image with a spatial resolution of 2.4 m was used.

Meteorological and climatic data measured at the North Tehran station, including air temperature, pressure, relative humidity, wind speed, and incoming radiation, were used for this study. The time of recording the weather and climate data used in the study was simultaneous with the moment of the satellite's passage from the area under the study. The location of the meteorological station is illustrated in Fig. 1.

For evaluating and comparing the accuracy of normalized and modeled LST of different models, soil temperature recorded by ground-based devices at the moment of satellite passage was used. The geographic location of each data logger of soil temperature is shown in Fig. 1. The locations of the data loggers were chosen to cover different topographic conditions. The data logger model for soil temperature used in this study was Eletich RC-5. Twelve of these devices were placed at a depth of 1 cm of the soil and continuously recorded soil temperature for 20 days (15 August 2017 to 05 September 2017). The accuracy of soil temperature recording by these devices was 0.5 °C for the temperature range of −20 °C–40 °C, and 1 °C for outside the temperature range. The locations of the data loggers were determined using a handheld GPS with an error of less than 6 m.

2.3. Method

This study aimed at developing and comparing the efficiency of physical models based on energy balance equations for normalization of LST relative to environmental parameters. In the first step, a dual-EB model was developed for vegetation and soil fraction covers with regional and local optimization strategies for modeling and normalization of LST, respectively. In the second step, a triple-EB model was developed for vegetation, soil, and built-up land fractional covers with regional and local optimization strategies, respectively. In the third step, the accuracy of modeling results and normalization of LST from different models were evaluated and compared. The correlation coefficient and RMSE between the modeled LST values and those obtained from the satellite image and the soil temperature measured by data loggers were computed. In addition, the variance of normalized LST values was calculated and analyzed.

2.3.1. Preprocessing and calculating LST

Atmosphere correction was conducted by the use of the Fast Line-of-sight Atmospheric Analysis of Hypercubes (FLAASH) algorithm (Cooley et al., 2002) owing to the importance of radiometric and atmospheric effects on the final result of LST. This module employed the MODTRAN 4 model which utilized the time of satellite's passage, the sensor's elevation, the geographical position of the study area, solar radiation angle, and the atmospheric model of the region (Cooley et al., 2002). The downloaded data from the USGS included the Landsat Level-1 Precision Terrain (L1TP) data which are considered suitable for time-series analysis. The geo-registration was consistent and the root mean square error (RMSE) less than 12 m was achieved. The geometric correction of image-to-image was conducted to match Landsat 8 image and GDEM.

A systematic methodology is required to estimate LST from the Landsat data. The DN (digital number) value of pixels was converted into at-sensor spectral radiance (L_s) as a preparatory step for thermal image processing. By the use of the inverted Planck's Law with an assumption that the Earth's surface is a black body with an emissivity value equal to 1 (Li et al., 2011; Walawender et al., 2014), the at-sensor spectral radiance was converted to at-sensor brightness temperature (T_s). Finally, LST was calculated from Landsat 8 using the Single Channel (SC) (Yu et al., 2014; Jiménez-Muñoz et al., 2014) and the Split Window (SW) (Jiménez-Muñoz et al., 2014) algorithms.

For LST retrieval, a SC LST estimation algorithm (Walawender et al., 2014; Sobrino et al., 2004) (Eq. (1)) was applied.

$$LST = \gamma\left[\frac{1}{\varepsilon}(\psi_1 L_s + \psi_2) + \psi_3\right] + \delta \tag{1}$$

where ε is land surface emissivity (LSE) and γ and δ are the Planck's function-dependent parameters, which can be estimated through Eqs. (2) and (3) (Farifteh et al., 2007):

$$\gamma = \frac{T_s^2}{b_\lambda L_s} \tag{2}$$

$$\delta = L_s - \frac{T_s^2}{b_\lambda} \tag{3}$$

where b_μ is 1324 K and λ stands for the effective wavelength of the thermal bands (λ = 10.904 for Landsat 8/TIRS B1).

The applied SC algorithm was unique as it incorporated atmospheric correction and considered different emission properties of the surfaces. ψ_1, ψ_2, and ψ_2 are the atmospheric functions related to the water vapor content of the atmosphere. They can be calculated by the use of Eq. (4) (Farifteh et al., 2007; Fernández-Espinosa, 2016):

$$\delta = -\gamma \times L_s + T_s \tag{4}$$

The obtained water vapor data in this study were from the MOD07 water vapor data product.

The SW technique uses two TIR bands typically located in the atmospheric window between 10 and 12 μm. The basis of the technique is that the radiance attenuation for atmospheric absorption is proportional to the radiance difference of simultaneous measurements at two different wavelengths, each of them being subject to different amounts of atmospheric absorption. For LST retrieval, a SW LST estimation algorithm (Jiménez-Muñoz et al., 2014) (Eq. (5)) was applied.

$$LST = T_i + c_1(T_i + T_j) + c_2(T_i - T_j)^2 + c_0 + (c_3 + c_4\omega)(1-\bar{\varepsilon}) + (c_5 + c_6\omega)\Delta\varepsilon \tag{5}$$

where T_i and T_j are the at-sensor brightness temperatures at the SW bands i and j (in kelvins), $\bar{\varepsilon}$ is the mean emissivity, $\bar{\varepsilon} = 0.5(\varepsilon_i + \varepsilon_j)$, Δε is the emissivity difference, $\Delta\varepsilon = (\varepsilon_i - \varepsilon_j)$, w is the total atmospheric water vapor content, and c_0 to c_6 are the SW coefficients to be determined from simulated data (Jiménez-Muñoz et al., 2014).

The retrieved land surface emissivity (LSE) data by the normalized difference vegetation index threshold method (NDVIT) is an easy-to-use method for calculating LSE (Kalogirou, 2013; Farifteh et al., 2007; Fernández-Espinosa, 2016). The NDVIT used thresholds to distinguish among soil pixels (NDVI < NDVIs), pixels of full vegetation (NDVI > NDVIv) and mixed pixels of soil and vegetation (NDVIs ≤ NDVI ≤ NDVIv). For this research, the values of NDVIs = 0.2 and NDVIv = 0.5 were used as proposed by Reference (Fernández-Espinosa, 2016) for the universal condition. Next, the threshold values were used to calculate the proportion of vegetation (PV) (Eq. (6)), and the result was

imported to the LSE algorithm (Fernández-Espinosa, 2016).

$$P_v = \left(\frac{NDVI - NDVI_s}{NDVI_v - NDVI_s}\right)^2 \quad (6)$$

The corrected emissivity of bare soil (εsλ) and full vegetation (εvλ) pixels were set to 0.96 and 0.99, respectively (Sobrino et al., 2004; Sobrino et al., 2008). A new emissivity value of 0.995 for water bodies was fixed after considering the very low reflectance of water bodies in the thermal infrared spectral range (Walawender et al., 2014). The emissivity for the mixed pixel (NDVIs ≤ NDVI ≤ NDVIv) was calculated by the use of Eq. (7) (Sobrino et al., 2004; Sobrino et al., 2008).

$$\varepsilon = \varepsilon_{v\lambda} \times P_v + \varepsilon_{s\lambda} \times (1 - P_v) + C_\lambda \quad (7)$$

where C_λ is the estimated correction factor for decreasing the cavity effect due to the surface roughness. C_λ was computed by Eq. (8).

$$C_\lambda = (1 - \varepsilon_{s\lambda}) \times \varepsilon_{v\lambda} \times F' \times (1 - P_v) \quad (8)$$

Depending on the surface distribution, F′ is the geometrical factor. The mean value of rough and heterogeneous surface $F' = 0.55$ was fixed (Rapaport et al., 2015).

The accuracy of LST values obtained from each algorithm was evaluated and compared using soil temperature data recorded by ground-based devices at the moment of the satellite's passage.

2.3.2. Environmental parameters

Both topographic conditions and incoming radiation are important factors influencing LST. In order to accurately model LST and normalize it, incoming radiation must be calculated to the surface on a pixel scale (Malbéteau et al., 2017). Incoming radiation to the surface is a collection of direct and diffuse solar radiation from sky and direct and diffuse radiation reflected from nearby terrains (Dubayah, 1994). The value of this parameter depends on a set of factors such as sky cloudiness, atmospheric conditions and parameters, time in a day and date in a year, geographical latitude and longitude, albedo of nearby terrains surface, and nearby terrains topography (Cooley et al., 2002). Details for calculating the incoming radiation to the surface can be found in (Kalogirou, 2013).

The other parameter affecting LST variations was the effect of ELR. The ELR effect indicates that in the troposphere with a constant spatial and time position, an increase in the elevation of the sea's surface reduces air pressure. This action is conducted adiabatically as internal air energy is reduced and the temperature is lowered. When a parcel of air expands, it pushes on the air around it, doing work (thermodynamics). Since the parcel does work but gains no heat, it loses internal energy so that its temperature decreases (Jacobson, 2005). The value of this parameter should be determined according to each spatial and temporal position. In order to model the ELR effect, the GDEM of the study area was used in the proposed model.

Among the most important parameters affecting LST were surface biophysical characteristics such as albedo, greenness and wetness. Landsat 8 bands were used to model surface biophysical characteristics. To this aim, these bands were first corrected using the modified cosine correction method (Hantson & Chuvieco, 2011; Richter et al., 2009) relative to the topographic effect. Then, biophysical parameters such as wetness were modeled based on the tasseled cap transformation for Landsat 8 (Liu et al., 2014; Liu et al., 2015), NDVI (Tucker, 1979) and albedo (Weng et al., 2004; Silva et al., 2016).

2.3.3. Energy balance models for normalization of LST

It is essential to obtain the temperature of the different fractional covers for normalizing LST based on energy balance equations. For areas including bare soil and vegetation covers, calculation of temperature of dry bare soil, wet bare soil, fully-stressed vegetation and unstressed vegetation were required. The proposed method for normalization of LST based on dual-EB model for areas with fractional vegetation and soil covers is shown in Fig. 2.

In the areas where built-up land fraction co-existed with fractional vegetation and soil covers, the energy balance equations were separately formed for built-up lands, and temperatures of the dry and wet built-up lands were calculated. By combining the calculated temperature values for each of the fractional covers, LST at the pixel scale was estimated. Eventually, based on the modeled and calculated LST from the satellite image, normalized LST was obtained. The LST obtained from Landsat 8 is a plot of all surface energy balance components such as net radiation flux, soil heat fluxes, sensible heat flux, latent heat flux and geothermal heat flux. In this paper, the components net radiation flux, soil heat fluxes, sensible heat flux and latent heat flux are modeled according to the characteristics of different surface covers. Then, according to these components, the LST of the region is modeled. The modeled LST does not include the effects of the geothermal heat flux component. Therefore, by subtracting the observed LST from the Landsat image and the modeled LST, normalized LST, including geothermal heat flux, was obtained. After normalizing the LST, the effects of net radiation flux, soil heat fluxes, sensible heat flux and latent heat flux were removed from the LST of the pixels.

The proposed method for normalizing LST based on three-dimension energy balance equations with fractional soil and vegetation covers, and built-up land is illustrated in Fig. 3.

Dry bare soil, wet bare soil, fully stressed and unstressed vegetation extreme temperatures were then derived by solving the EB equations for each case, as described Eqs. (9), (10), (11), (12), (13) and (14) equations, respectively (Malbéteau et al., 2017; Merlin & Chehbouni, 2004; Anderson et al., 2008; Long & Singh, 2012; Merlin et al., 2005; Merlin et al., 2010).

$$Rn_{s,dry} - G_{dry} = H_{s,dry} \quad (9)$$

where $Rn_{s,\,dry}$ (W/m^2) is the net radiation for dry soil, G_{dry} (W/m^2) the ground heat in dry condition and $H_{s,\,dry}$ (W/m^2) the sensible heat of dry soil.

$$Rn_{s,wet} - G_{wet} = H_{s,wet} + LE_{s,wet} \quad (10)$$

where $Rn_{s,\,wet}$ (W/m^2) is the net radiation for wet soil, G_{wet} (W/m^2) the ground heat in wet condition, $H_{s,\,wet}$ (W/m^2) the sensible heat of wet soil and $LE_{s,\,wet}$ (W/m^2) the latent heat of wet soil.

$$Rn_{v,dry} = H_{v,dry} \quad (11)$$

where $Rn_{v,\,dry}$ (W/m^2) and $H_{v,\,dry}$ (W/m^2) are the net radiation and the sensible heat of water-stressed vegetation, respectively.

$$Rn_{v,wet} = H_{v,wet} + LE_{v,wet} \quad (12)$$

where $Rn_{v,\,wet}$ (W/m^2), $H_{v,\,wet}$ (W/m^2) and $LE_{v,\,wet}$ (W/m^2) are net radiation, sensible heat, and latent heat flux of unstressed vegetation, respectively.

$$Rn_{Imp,dry} - G_{dry} = H_{Imp,dry} \quad (13)$$

where $Rn_{Imp,\,dry}$ (W/m^2) are net radiation for dry built-up land, G_{dry} (W/m^2) the ground heat in dry condition and $H_{Imp,\,dry}$ (W/m^2) the sensible heat of dry built up land.

$$Rn_{Imp,wet} - G_{wet} = H_{Imp,wet} + LE_{Imp,wet} \quad (14)$$

where $Rn_{Imp,\,wet}$ (W/m^2) are the net radiation for wet built up land, G_{wet} (W/m^2) the ground heat in wet condition, $H_{Imp,\,wet}$ (W/m^2) the sensible heat of wet built up land and $LE_{Imp,\,wet}$ (W/m^2) the latent heat of wet built up land. The expressions of each flux component of the above EB equations can be found in (Malbéteau et al., 2017; Merlin & Chehbouni, 2004; Anderson et al., 2008; Long & Singh, 2012; Merlin

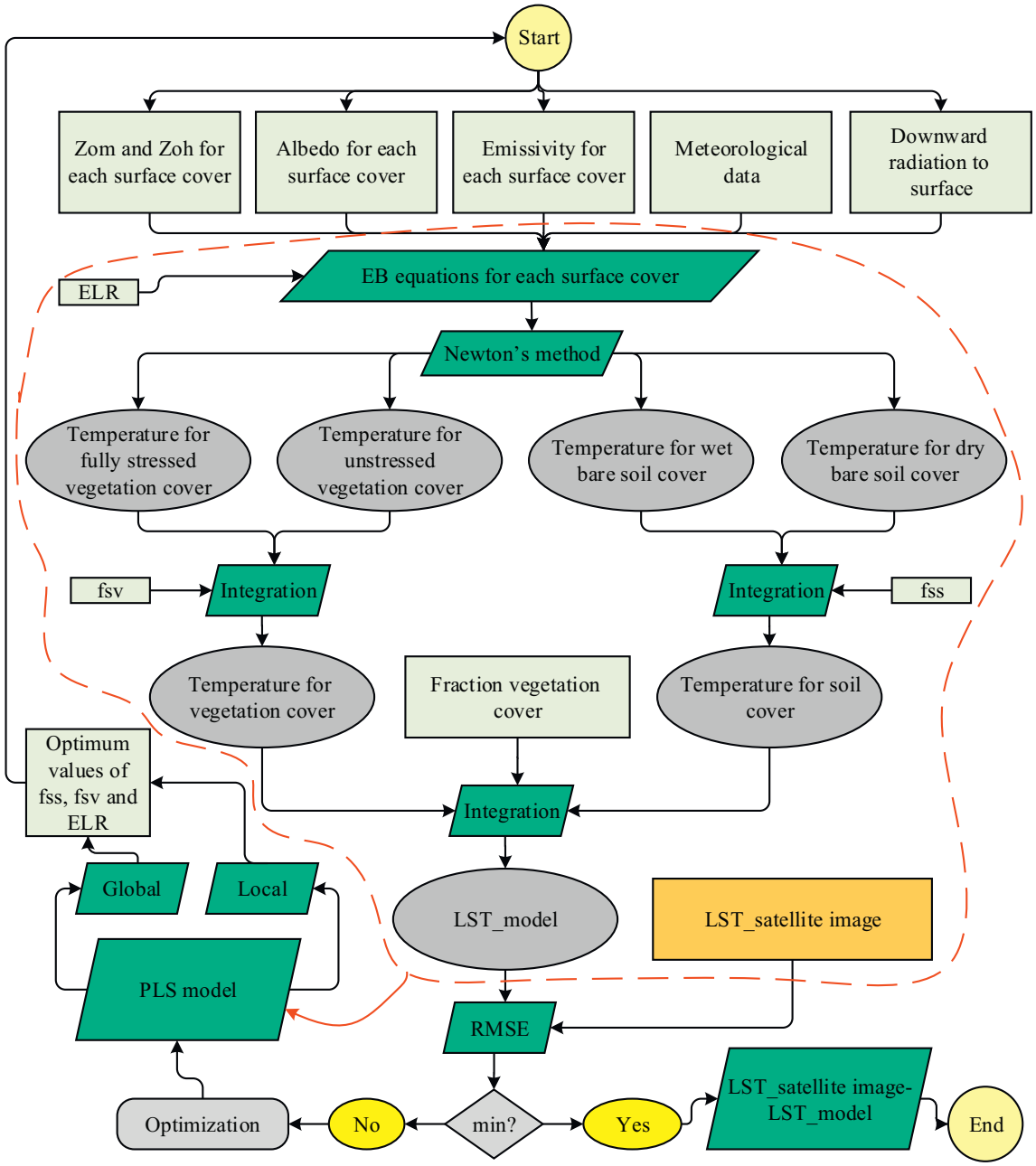

Fig. 2. The regional and local dual-EB models for normalization of LST.

et al., 2005; Merlin et al., 2010; Choudhury et al., 1986; Stefan et al., 2015; Bristow, 1987).

Air temperature (Ta) at the pixel scale was estimated per Eq. (15) (Malbéteau et al., 2017).

$$T_a = T_{station} + ELR(E - E_{station}) \quad (15)$$

where $T_{station}$ (°C) is air temperature measured at the North Tehran meteorological station, E (m) the pixel elevation, $E_{station}$ (m) the elevation of the station, and ELR the environmental lapse rate (°C/m). The latter is defined as the rate at which air temperature decreases with increasing elevation. ELR was estimated at the image scale for Landsat overpass date.

The temperature for dry bare soil, wet bare soil, fully stressed, unstressed vegetation, dry built-up land and wet built up land were estimated using the Newton's method (Bristow, 1987).

Bare soil temperature at the pixel scale was calculated with Eq. (16) (Malbéteau et al., 2017).

$$Ts_{EB} = fss \times T_{s,dryEB} + (1 - fss) \times T_{s,WetEB} \quad (16)$$

where Ts_{EB} is soil temperature at the pixel scale in °C, $T_{s,\ dryEB}$ in °C soil temperature in dry condition at the pixel scale, $T_{s,\ WetEB}$ in °C the soil temperature in wet condition at the pixel scale and fss a dryness index of the soil surface. The fss equals to 1 when the soil is fully dry (surface soil moisture close to the residual value) and to 0 when the soil is fully wet (surface soil moisture close to the soil moisture at saturation).

Vegetation temperature at the pixel scale was calculated with Eq. (17).

$$Tv_{EB} = fsv \times T_{v,dryEB} + (1 - fsv) \times T_{v,WetEB} \quad (17)$$

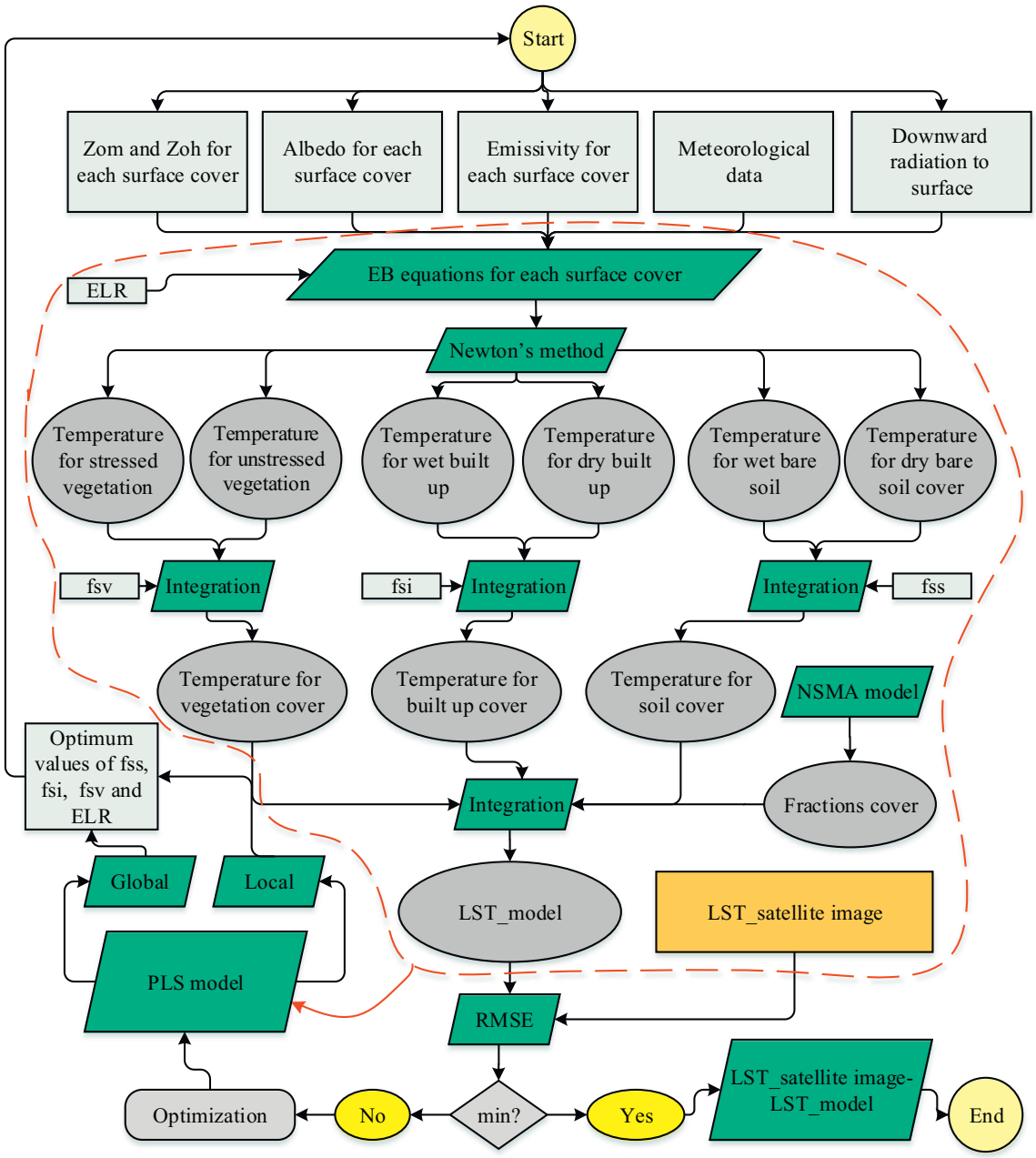

Fig. 3. The regional and local triple-EB models for normalization of LST.

where Tv_{EB} is vegetation temperature on pixel scale in °C, $T_{v,\ dryEB}$ is temperature of fully stressed (non-transpiring) vegetation at the pixel scale in °C, $T_{v,\ WetEB}$ is temperature of vegetation that is unstressed (transpiring at the potential rate) at the pixel scale in °C, and fsv is vegetation water stress index. fsv equals to 1 when the root zone soil moisture is above field capacity and 0 when the root zone soil moisture is below the wilting point.

Built up land temperature at the pixel scale was calculated with Eq. (18).

$$T_{ImpEB} = fsi \times T_{Imp,dryEB} + (1-fsi) \times T_{Imp,WetEB} \quad (18)$$

where T_{ImpEB} is built up land temperature at the pixel scale in °C, $T_{Imp,\ dryEB}$ is built up land temperature in dry condition at the pixel scale in °C, $T_{Imp,\ WetEB}$ is built up land temperature in wet condition at the pixel scale in °C, and fsi a dryness index of built up surface. fsi equals to 1 when the built up is fully dry (surface built up moisture close to the residual value) and to 0 when the built up is fully wet (surface built up moisture close to the built up moisture at saturation).

The modeled and normalized LST were calculations based on the dual-EB model using Eqs. (19) and (20):

$$T_{2EB} = f_v \times T_{vEB} + (1-f_v) \times T_{sEB} \quad (19)$$

$$T_{2Correct} = LST - T_{2EB} \quad (20)$$

where T_{2EB} is the modeled LST of the dual-EB model at the pixel scale in °C, $T_{2Correct}$ is the normalized LST at the pixel scale in °C, and f_v is the fractional vegetation cover at the pixel scale.

The modeled and normalized LST were calculated based on the triple-EB model using Eqs. (21) and (22):

$$T_{3EB} = f_S \times T_{sEB} + f_V \times T_{vEB} + f_{Imp} \times T_{ImpEB} \quad (21)$$

$$T_{3Correct} = LST - T_{3EB} \quad (22)$$

where T_{3EB} is the modeled LST of the triple-EB model at the pixel scale in °C, $T_{3Correct}$ is the normalized LST of the triple-EB model at the pixel scale in °C, and f_s and f_{Imp} are the fractional soil cover and fractional impervious cover at the pixel scale, respectively.

The normalized spectral mixture analysis (NSMA) model (Wu, 2004) was employed to extract fractional covers of bare soil, vegetation and built-up. To evaluate the accuracy of the fractional cover maps, the image of the WorldView 2 was used. The correlation coefficient and RMSE between the fractional covers obtained from the Landsat 8 image and the areal ratios for each of these covers on the WorldView 2 satellite image were calculated and analyzed for the selected 60 pixels of the samples. There samples were selected to represent different surface characteristics.

Given that Landsat LST observations were available to calibrate the environmental parameters normalization model, three additional constraints were applied to the LST model in Eqs. (19) and (21). The first step minimized the mean difference between observed and modeled LST by using Eq. (23):

$$T_{EB} = \overline{LST} + T_{EBmodel} - \overline{T_{EBmodel}} \quad (23)$$

where $\overline{LST}$ is the mean of LST obtained from satellite image, $T_{EBmodel}$ is the modeled LST at the pixel scale, and $\overline{T_{EBmodel}}$ is the mean of modeled LST for the region.

The second step consisted in adjusting fss, fsv and fsi by minimizing the RMSE between LST obtained from satellite image and modeled LST. The third step adjusted ELR in Eq. (15) by minimizing the RMSE between LST obtained from satellite image and modeled LST. The above calibration needed initializing ELR with a ELR first-guess of −6 °C·km^{-}•, according to (Glickman & Zenk, 2000). In order to calculate the unknown parameters (fss, fsv, fsi and ELR) of relations Eqs. (16), (17) and (18) with the condition of minimizing the variance of normalized LST values, the PLS model was used (de Paulo et al., 2016; Farifteh et al., 2007; Fernández-Espinosa, 2016; Rapaport et al., 2015).

In this study, we considered two different approaches of regional and local optimization for solving the unknown parameters of the PLS model for normalization of LST. In the regional optimization strategy, the values of the entire dependent (LST obtained from satellite image) and the independent (dry bare soil, wet bare soil, fully stressed, unstressed vegetation, dry built-up land and wet built up land) variables were presented simultaneously to the PLS model and for f_{ss}, f_{sv} and f_{si}, an optimal value was calculated at the region scale. In the local optimization strategy, fss, fsv and fsi parameters were calculated individually. In this approach, for each pixel, only the values of the neighboring pixels of the dependent variable and the independent variables were introduced to the PLS model and the optimal values of fss, fsv and fsi were calculated at the pixel scale. The strategy of determining the optimal values of fss, fsv and fsi in the normalization model for regional and local optimization strategies is generally shown in Fig. 4.

2.3.4. The model accuracy evaluation

For the evaluation and comparison of the accuracy of the modeling results, the correlation coefficient and RMSE were computed between the modeled LST values and obtained from the satellite image. The purpose of LST normalization was to minimize the difference in LST due to the environmental parameters for different regions (pixels). The variance of a set of values denoted the amount of variation or fluctuation of the set values relative to the set average. Therefore, the variance of LST values, affected by heterogeneous environmental parameters, was high. Normalization of LST values relative to the environmental parameters reduced the temperature difference resulting from this parameter for different regions. As a result, the variance of normalized LST values reduced. For this reason, to evaluate the accuracy of LST normalization results, the variance of normalized LST values was calculated and analyzed. To confirm the efficiency of the normalization model, the correlation coefficient for LST and the environmental parameters were investigated before and after the normalization. Finally, to evaluate and compare the accuracy of the results of using the actual data, the correlation coefficient and RMSE were calculated and studied for the modeled LST and the measured soil temperature by the data loggers.

3. Results

3.1. Modeling environmental parameters

Following the preprocessing, environmental parameters, such as topography variables including the elevation, slope and aspect and biophysical variables including albedo, wetness and vegetation, were extracted by using GDEM and Landsat 8 image and the fractional covers of the region were calculated at the pixel scale using the NSMA model of 17 August 2017 (Fig. S1). The correlation coefficient and RMSE were calculated between the values of the fractional covers and the values of the areal ratios of each of these covers on the WorldView 2 satellite image for the selected 60 pixels of the samples (Fig. S2). Results of accuracy assessment indicated the high accuracy of the fractional cover maps were obtained from the NSMA model and the Landsat 8.

LST was calculated by using SW and SC algorithms for 17 August 2017. The accuracy of the results of each algorithm was evaluated by using soil temperature data recorded by ground-based devices (Fig. S3). Fig. S3 shows that the accuracy of the SC algorithm for calculating LST was higher. The heterogeneous topographic condition of the region was the main reason for the relatively large difference in LST. The incoming radiation to the surface at the moment of satellite passage was also modeled. The difference in the mean incoming radiation to the modeled and measured at the meteorological station at the moment of the satellite passage was less than 30 W/m^2, indicating the high accuracy of the modeled incoming radiation. The LST maps and incoming radiation to the surface at the moment of the satellite passage on 17 August 2017, are shown in Fig. S4.

Despite the overall low elevation of the study area, the range of changes in the incoming radiation to the surface was high, which was attributable to the mountainous condition and heterogeneous topography of the region.

3.2. Energy balance modeling results for normalization of LST with regional and local optimization

The temperature of the fractional dry and wet soil covers, fully stressed and unstressed vegetation covers and dry and wet built-up lands for 17 August 2017 were calculated, and are illustrated in Fig. S5. Dry soil cover possessed the highest LST due to the absence of latent heat flux. Wet bare soil and unstressed vegetation cover observed a lower LST. The mean LST of wet bare and dry bare soil yielded 31.3 °C and 46 °C, respectively. The significant reduction of wet soil temperature was due to evaporation and thus latent heat. The same thing shows the importance of considering all the components of the energy balance in the modeling and normalization of LST.

Given the different cover temperatures and LST obtained from satellite images, the optimal values of fss, fsv and fsi were determined, so that RMSE was minimized between the modeled LST and the observed LST from the satellite image. To this aim, the PLS model was used. Using the PLS model in the regional optimization strategy, an optimal value for the parameters fss, fsv, fsi and final ELR for 17 August 2017 were estimated for the whole region. The optimal values of these parameters are indicated in Table S2.

Eq. (15) was used to calculate ELR value. Theoretically, the ELR value is considered approximately in dry adiabatic condition, 9.8 degrees per km; in semi-dry adiabatic conditions, at an elevation lower than 10 km from the atmosphere, 7–6 degrees per km; and in wet adiabatic conditions 3.6 degrees per km (Danielson et al., 2003; Rolland, 2003; Minder

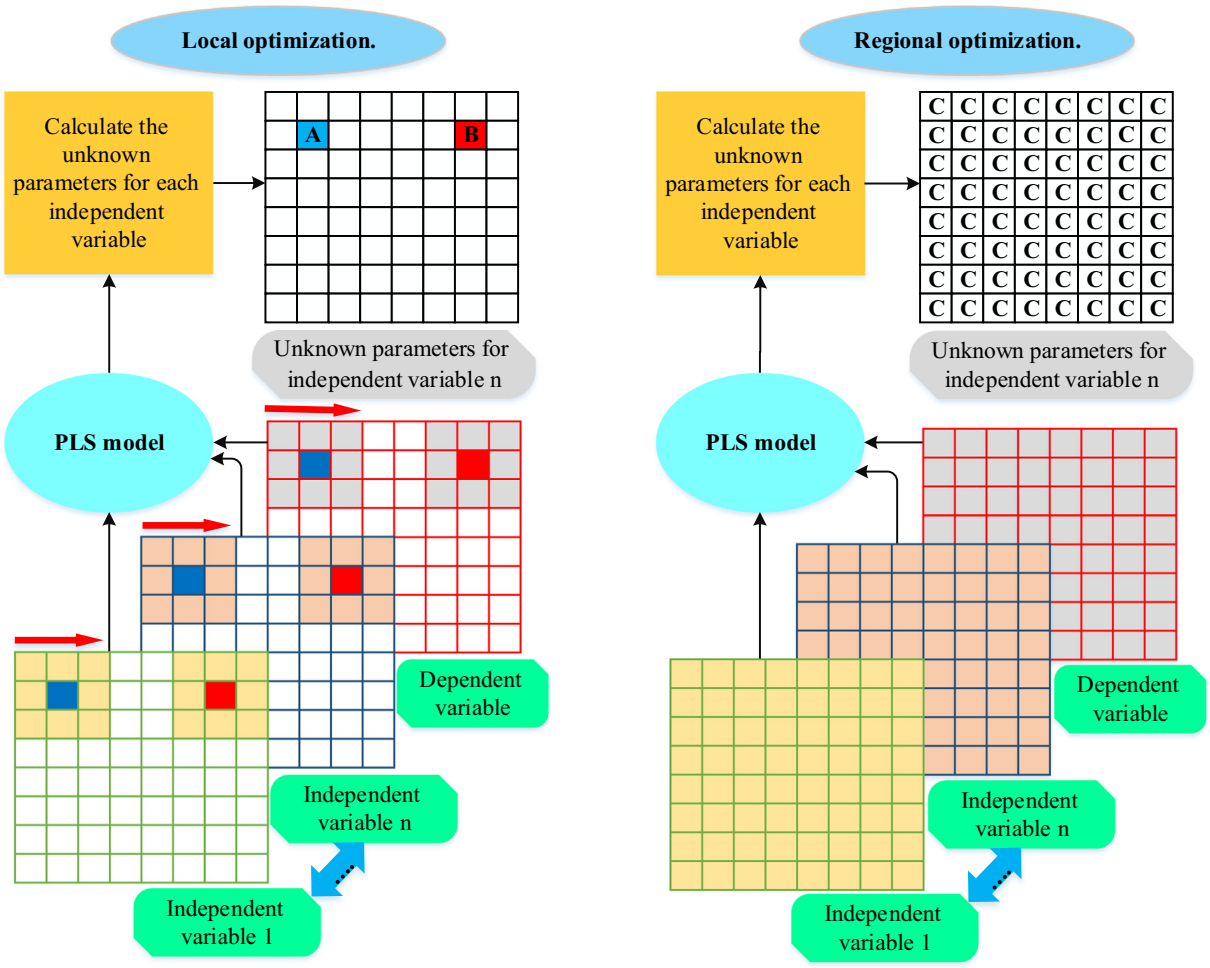

Fig. 4. Conceptual model for determining unknown parameters with regional (right) and local (left) optimization.

et al., 2010). Due to the high relative humidity on 17 August 2017, in the study area, ELR was close to 3.6. For the fss parameter, the value was greater than 0.5 due to dry and desert climate conditions, which implied dry conditions for the soil surface too. The value of the parameter fsv (more than 0.5) indicated the presence of water stress in vegetation. The value of fsi was greater than 0.5, indicating the dry conditions for the surface of the built-up lands.

By local implementation of the PLS model, the optimal values of fss, fsv and fsi for 17 August 2017 were calculated at the pixel scale (Fig. S6). By calculating the optimal values of the parameters, regionally and locally, the soil, vegetation and built-up lands covers temperatures for 17 August 2017 were calculated. The results of modeled LST by using dual-EB and triple-EB models in the regional and local optimization strategies are shown in Fig. 5.

The modeled LST maps with regional optimization strategy show that when only two fractional covers, soil and vegetation, were used for estimation, LST of built-up lands located in the south of the study region was modeled higher than the real values and similar to LST of soil cover. Based on the LST map obtained from the Landsat 8 image of the study area, the LST of built-up land was lower than that of soil cover. The reason is that by using two fractional covers of soil and vegetation, areas with built-up lands were considered as soil cover, and the equivalent temperature to the soil temperature was modeled for them, but such areas indeed had different soil temperature from soil. When three fractional covers, soil, vegetation, and built-up land of 17 August 2017 were used for estimation, LST of the built-up lands decreased.

Fig. 5 shows that the effect of environmental parameters was significantly normalized from the values of the LST obtained from the satellite images. By LST normalization to environmental parameters, the heterogeneous distribution of LST obtained from the satellite images for the region has been reduced. The normalized LST maps indicate that the use of local optimization strategy reduced the effects of different parameters much better than the regional optimization on LST. Adding of built up into the energy balance equations were effective in reducing the effects of various parameters of LST obtained from the satellite image. In order to evaluate the accuracy of the models, the relationship between the modeled LST and observed LST obtained from Landsat 8 was assessed, and the correlation coefficient and the RMSE between two parameters were calculated. Furthermore, the variance of normalized LST for each model to17 August 2017 was calculated. The result of the evaluation of the models is shown in Fig. 6.

The modeling results show that the use of the Triple-EB model for normalizing LST increased the accuracy compared to the Dual-EB model. When the fraction of built-up land was incorporated, RMSE reduced between the modeled LST and observed LST from Landsat 8, as well as the variance of normalized LST. These reductions were by 0.47 and 2.7 with the regional optimization, respectively, and by 0.64 and 0.285, with the local optimization, respectively. However, the variation in the values of variance of normalized LST was not high and accurate. The most important reason for this improvement of modeling was the complexity of the built-up land. The heterogeneity of the built-up land with respect to the biophysical, texture and morphology properties

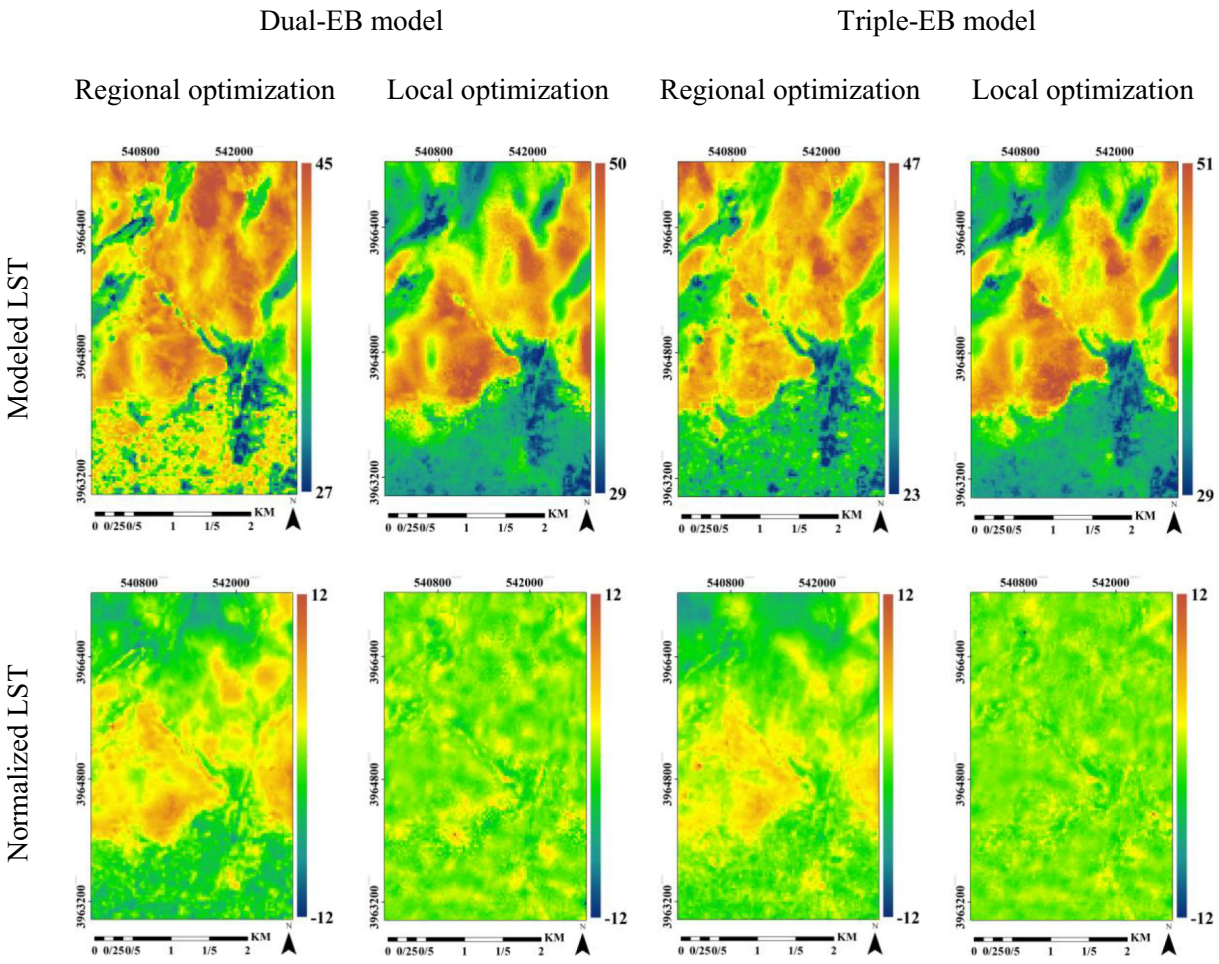

Fig. 5. The results of modeled and normalized LST (°C) on 17 August 2017.

made it difficult for modeling the surface energy balance. Among the morphological parameters of the built-up areas that affected the surface energy balance were surface roughness and momentum roughness length. This parameter was highly variable in urban environments (Jiang & Weng, 2017). Furthermore, for the energy balance of the built-up areas, anthropogenic heat flux should also be considered (Zheng & Weng, 2018). This factor directly affected the modeling of LST.

3.3. Evaluation of the modeling accuracy by using ground-based soil temperature data

To evaluate the performance of modeling results, modeled and normalized LST were compared with soil temperature data measured by ground-based devices. The correlation coefficient and RMSE were calculated between the modeled and measured LST, and the results are shown in Fig. 7. In addition, the variance of LST values measured by ground-based devices and normalized LST values with different models in the geographic locations of soil temperature measurement devices for 17 August 2017 were calculated, and the results are shown in Fig. 8.

Figs. 7 and 8 show that for LST modeling and normalization, the local optimization strategy had a higher efficiency than the regional optimization strategy. Modeling and normalization of LST were more efficient when three fractions of vegetation, soil, and built-up were considered than when only two fractions of vegetation and soil were considered. For energy balance modeling with the regional optimization, RMSE between modeled and measured LST yielded 6.56 for two fractions and 6.41 for three fractions, respectively. The variance of LST values measured by the ground devices was 5.73. This value was reduced after normalizing the LST relative to the environmental parameters. The lowest value of the variance for the normalized LST values in the geographic locations of the data loggers was achieved by the triple-EB model with the local optimization. Finally, to evaluate the efficiency of the best model presented in this study for LST normalization relative to environmental parameters, the relationship between LST and environmental parameters for 17 August 2017 was investigated before and after the normalization, and the results are shown in Fig. 9.

Results show the efficiency of the model to normalize LST relative to environmental parameters. For all of the environmental parameters, the coefficient was close to zero between the environmental parameters and the normalized LST. In other words, normalized LST was completely independent of the environmental parameters considered by this research.

To evaluate and validate the performance of the LST normalization models, Landsat 8 images for 30 Jun 2017, and 02 September 2017 were also used. Due to the limited research volume, only the final results are shown in Table S3.

Table S3 shows that for both 30 Jun 2017 and 02 September 2017, the use of local optimization strategy increased the accuracy of the normalization of LST, compared to the regional optimization strategy. In addition, no matter the regional or local optimization strategy was employed, the triple-EB model out-performed consistently the dual-EB model for LST normalization.

4. Discussion

LST derived from thermal remote sensing is of great importance in variety of applications such as ground and underground resources (Jia et al., 2017; Mansor et al., 1994), monitoring environmental

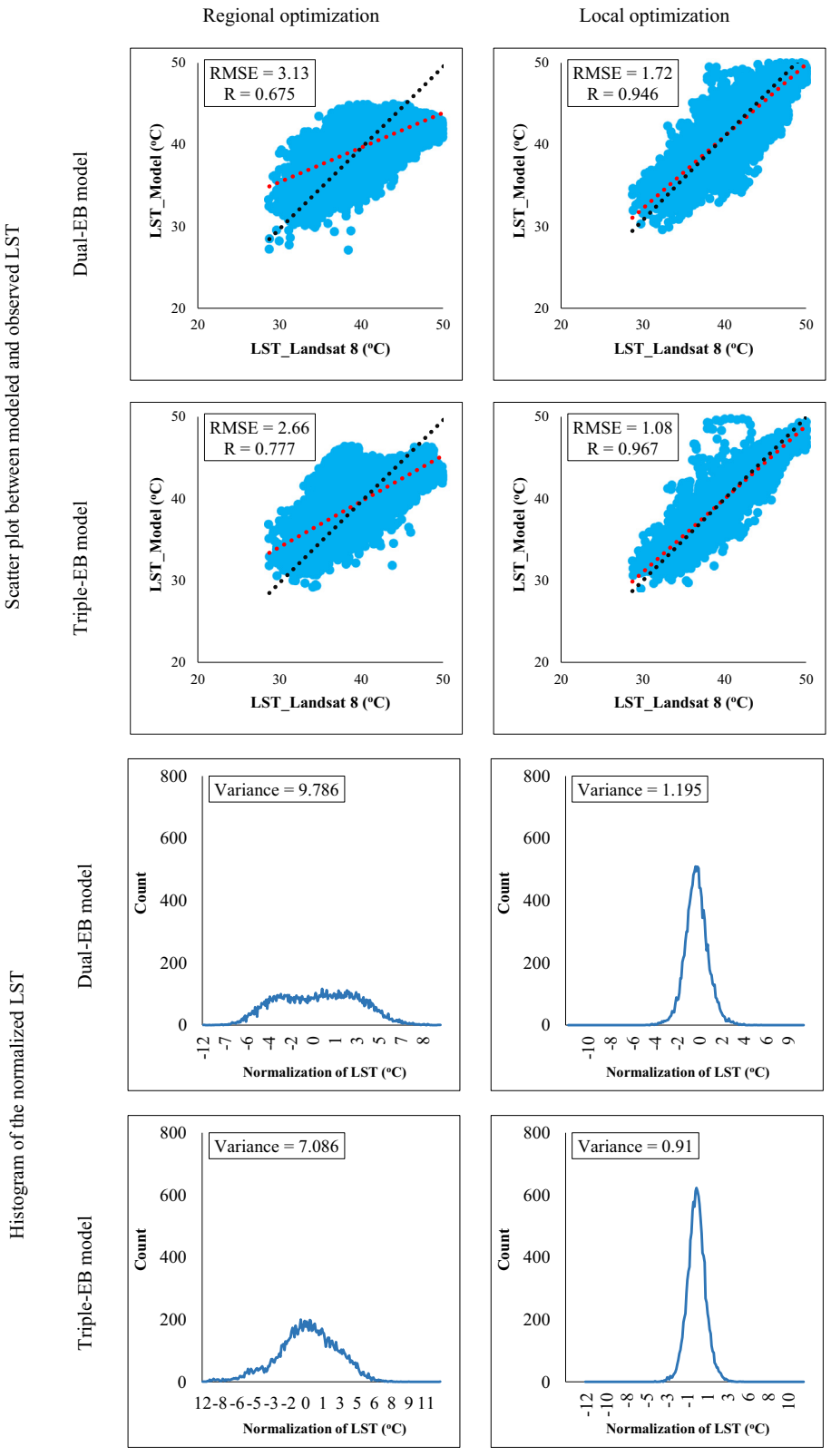

Fig. 6. RMSE and correlation coefficient between modeled and observed LST and the variance of normalized LST for each model on 17 August 2017.

phenomena (Wan et al., 2004), energy balance (Friedl, 2002) and geological structure Studies (Ma et al., 2010), climate change and urban phenomena (Okalebo et al., 2016; Voogt & Oke, 2003; Berger et al., 2017; Weng et al., 2004; Firozjaei et al., 2018; Panah et al., 2017), water resources management, surface moisture and evapotranspiration (Jia et al., 2017; Harris et al., 2017; Lievens et al., 2017) and various phenomena detection (Bellaoui et al., 2017; Eckmann et al., 2008). The surface temperature of the phenomena and the various complications in a natural and free environment is different due to the parameters such as time and geographical location, topographic conditions, inherent characteristics, biophysical characteristics, synoptic and climatic factors, and underlying conditions. Normalization of surface temperature

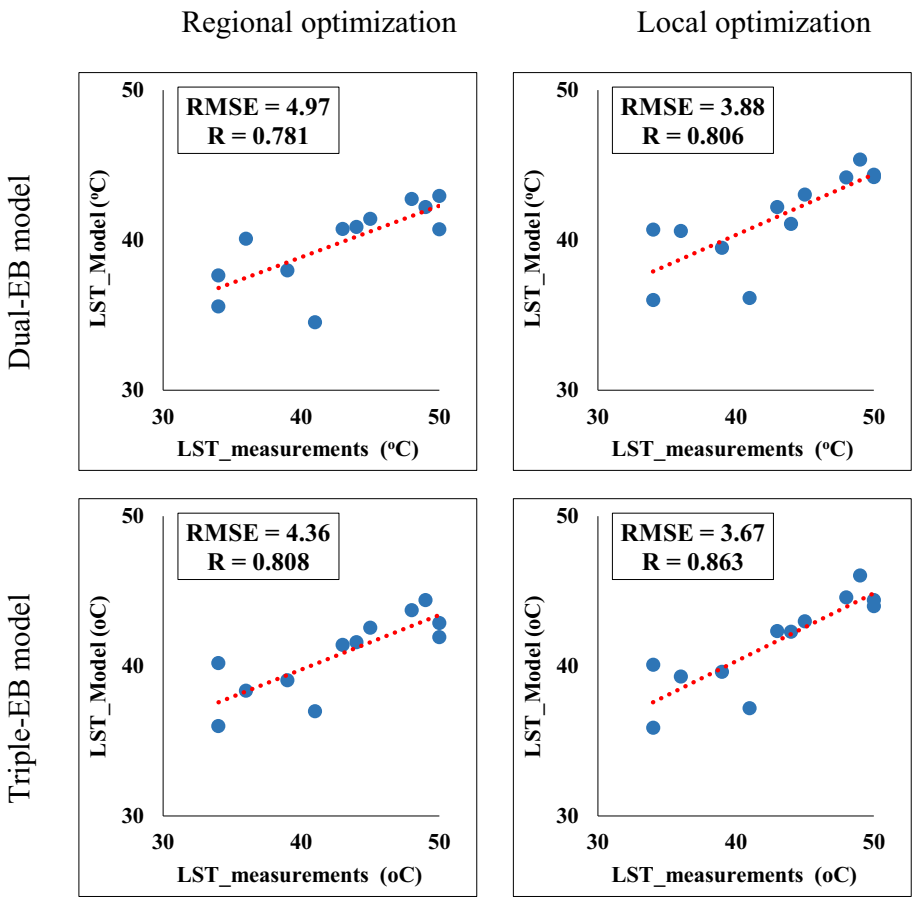

Fig. 7. Correlation coefficient and RMSE between the modeled LST and soil temperature measured by data loggers on 17 August 2017.

relative to environmental parameters is of significant importance in many scientific studies and managerial decisions such as identifying geothermal energy sources, monitoring the process of changes in the activity of faults and volcanoes, the trend of changes in thermal anomalies and their relationship with the land Seismicity in the non-urban environment and management and planning of energy use in urban environments (Coolbaugh et al., 2007; Gutiérrez et al., 2012; Malbéteau et al., 2017; Mattar et al., 2014).

In the past, studies have been done on the extent and quality of the effect of various environmental parameters on the amount of LST and the normalization of LST values is performed relative to mentioned parameters (Coolbaugh et al., 2007; Gutiérrez et al., 2012; Malbéteau et al., 2017; Dozier & Outcalt, 1979; Rigon et al., 2006; Jain et al., 2008; Chen et al., 2009; Peters et al., 2012; Benz et al., 2017).

Dozier and Outcalt (1979) used EB equations for simulation of LST in mountainous terrain. In this model, set of environment parameters were considered. However, this model was suitable only for arid and dry areas. In that study, for modeling the downward solar radiation, the direct and indirect reflection from adjacent terrains were considered. Also, the variation of air temperature with elevation was estimated using the standard ELR of $-6.5\ °C \cdot km^{-1}$, which is not constant in different regions and should be calculated for each region individually (Dozier & Outcalt, 1979). In this study, for modeling of downward solar radiation a collection of direct and diffuse solar radiation from sky and

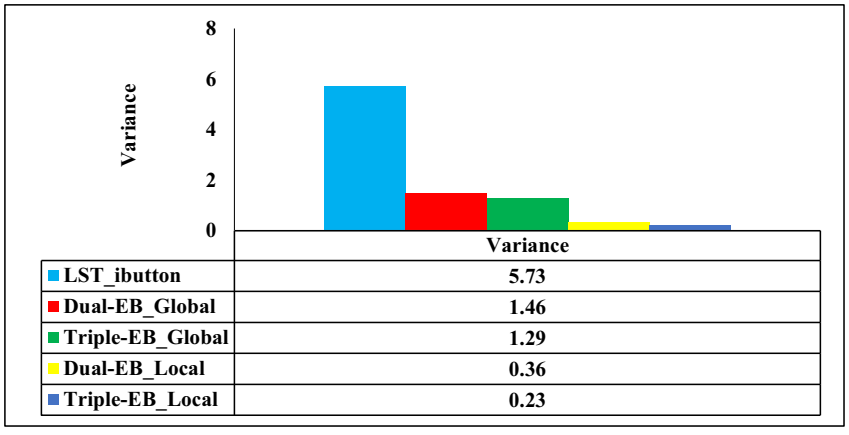

	Variance
LST_ibutton	5.73
Dual-EB_Global	1.46
Triple-EB_Global	1.29
Dual-EB_Local	0.36
Triple-EB_Local	0.23

Fig. 8. Variance of soil temperature and normalized LST with different strategies in the geographic locations of data loggers on 17 August 2017.

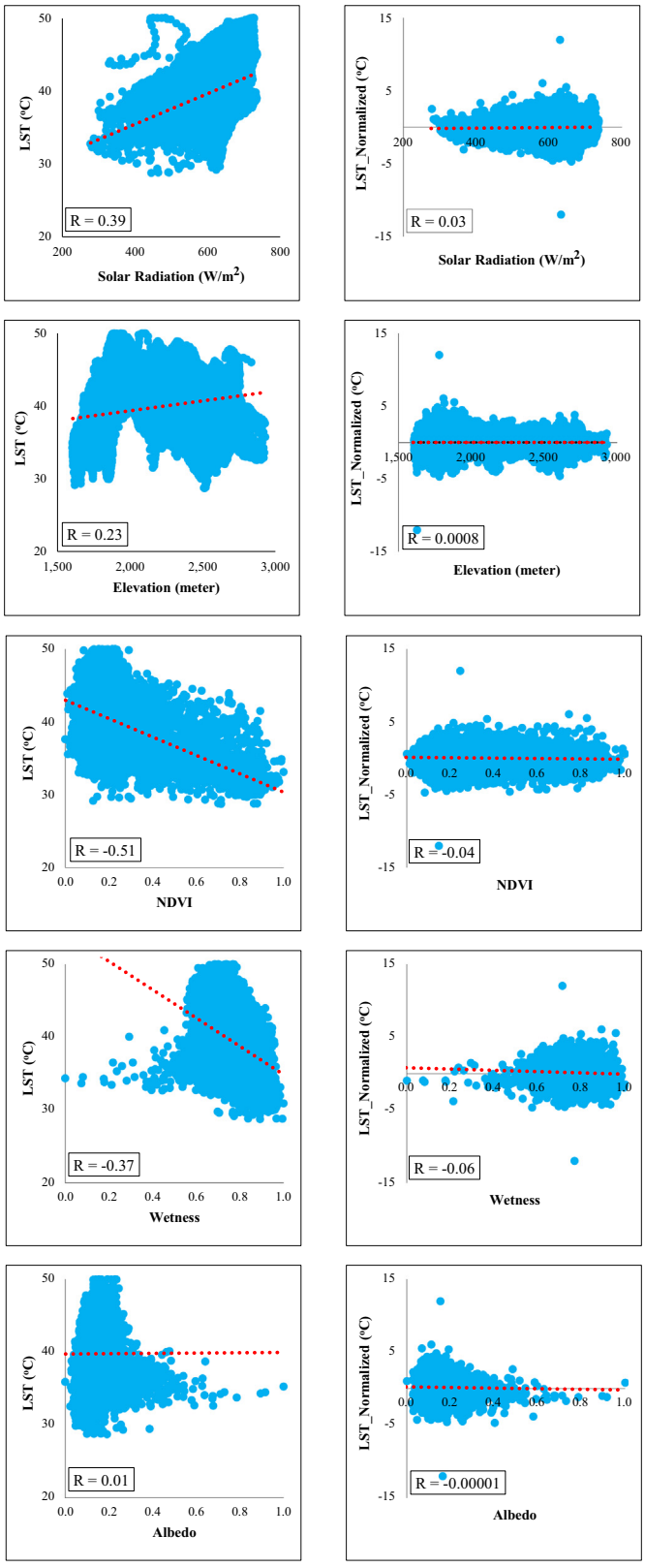

Fig. 9. Correlation coefficient between LST and environmental parameters before and after the normalization on 17 August 2017.

direct and diffuse radiation reflected from nearby terrains were considered. Further, for the parameter ELR, the optimal value for the study area was calculated (Table S2).

In Coolbaugh et al. (2007) study, LST obtained from thermal images was normalized relative to the environment parameters such as effects of topography parameters, surface albedo, surface emissivity and thermal inertia. Assuming that in arid and desert regions, the effects of sensible heat and latent heat flux parameters on LST were negligible, these two parameters were not included in the modeling. Therefore, the proposed model was inefficient for regions with substantial variations of biophysical characteristics (Coolbaugh et al., 2007). In current study, all components of the surface energy balance including net radiation, ground, sensible and latent heat fluxes were considered to normalization of LST.

In order to increase the efficiency of the model of the thermal anomalies detection for regions with high elevation changes, Gutiérrez et al. (2012) presented a linear model to consider the elevation effect on LST. The unknown parameters of the model were determined in a way that the variance of the normalized LST values be minimized; thus, the effect of the elevation parameter on the reduction of wrong anomalies was considered (Gutiérrez et al., 2012). In current study, the parameter of variance was used to evaluate normalized LST. The results of Fig. 9 show well that the normalized LST was independent from environmental parameters such as elevation, NDVI, solar radiation and albedo.

To normalized LST values relative to topographic parameters, Malbéteau et al. (2017) suggested three model of EB-based, multilinear regression, and slope of dry edges. ASTER images were used to evaluate the performance of the proposed methods. To determine the unknown parameters of the various models, the OLS and regional optimization were used. The normalization method was based on several assumptions. Both variables downward solar radiation and elevation were assumed independent from each other because the ML regression can only fit observed LST using a linear combination of independent variables. The correlation of independent parameters in modeling caused errors in the process of calculating the unknown coefficients of the model. Also, the energy balance equation model for normalizing the LST proposed considered only two fraction covers of vegetation and soil. For this reason it was not suitable for regions with three fraction covers of vegetation, soil and built-up lands (Malbéteau et al., 2017). In current study, to determine the unknown parameters of the various models PLS method was used. The PLS method allowed the use of dependent parameters and small number of samples in the model. For solving the unknown parameters in the normalization model, the local optimization strategy was proposed and calculated at the pixel scale. Results show that for LST modeling and normalization, the local optimization strategy had a higher efficiency than the regional optimization strategy. Further, a physical model based on energy balance equations was presented for three fractions of vegetation, soil and built-up land covers to modeling and normalization of LST relative to environment parameters.

The results of different parameters showed that the use of energy balance equations of three fractions of soil cover, vegetation and built-up lands increased the efficiency of the modeling over the two fractions of soil cover and vegetation. However, the difference between them was not significant. The most important reason for this insignificant difference was the complexity of the built-up land. High heterogeneity of the components of built-up lands in terms of biophysical, chemical, texture and morphology characteristics made it difficult to formulate and solve energy balance equations for the study area. The most important morphological parameters of the built-up areas affecting the energy balance equation were surface roughness, momentum roughness coefficient, wind speed, and air temperature near the surface (Jiang & Weng, 2017). These parameters were highly variable in the urban environments. Consequently, a fixed value for the whole built-up area may introduce a great deal of error into the model. In addition, for the energy balance modeling of built-up areas, anthropogenic heat flux should be considered along with other fluxes (Zheng & Weng, 2018).

In addition to the complexity and heterogeneity of built-up lands that made it difficult to solve the energy balance equations in the

urban environments, the efficiency of sub-pixel models can be considered to calculate the amount of different fractions of a pixel. The sub-pixel composition may have a direct effect on the amount of modeled and normalized LST and thus on heat fluxes (Weng et al., 2014). In mountainous areas, due to the complexity of topographic conditions, environmental parameters such as relative humidity, air pressure and wind speed vary changeable in spatial dimension. Due to the high sensitivity of components of the surface energy balance such as sensible and Latent heat flux in terms of relative humidity parameters, air pressure and wind speed, considering an average value for these parameters in the scale of the region causes an increase in the error in the modeling. In addition, the normalization model provided the ability to implement for thermal images with different spatial resolution. At present, there is a real limitation in the spatial resolution of thermal images. In the future, with the advancement of remote sensing technology and satellite spatial resolution of thermal images, better performance of the model proposed in this research can be expected.

5. Conclusions

LST obtained from thermal remote sensing have been used in various environment applications. The amount and spatial distribution of LST in a region is influenced by environmental parameters. The purpose of this study was to develop and compare physical models based on energy balance equations for normalizing LST relative to the environmental parameters. For this purpose, a set of remote sensing, meteorological, climatic, and land data were used. For modeling and normalization of LST, the physical model of dual-EB model for vegetation and soil fractions and triple-EB model for vegetation, soil and built up land fractions were developed with either regional or local optimization strategies. The distinction between this study and the previous studies in the context of normalization of LST obtained from satellite images lies in three areas: (1) A physical model based on energy balance equations was presented for three fractions of vegetation, soil and built-up land covers; (2) For solving the unknown parameters in the normalization model, the local optimization strategy was proposed and calculated at the pixel scale; and (3) To solve the unknown parameters related to the LST normalization model in relation to the environmental parameters, the Partial least-squares (PLS) method was used. The results indicated that in the energy balance model, the local optimization method outperformed the regional optimization method in the efficiency and accuracy of the normalization model. In the regional optimization method, the values of all pixels were simultaneously introduced into the PLS model, and for each unknown value, a common value was calculated for the entire pixels of the study area. In contrast, in the local optimization strategy, the unknown parameters were calculated separately for each pixel. For a specific pixel, the values of its nearby pixels were specified and the model was introduced to determine the optimal value of the unknown parameters for that pixel. LST normalization results show that the effect of environmental parameters had been significantly normalized from the values of the LST obtained from the satellite images. By LST normalization to environmental parameters, the heterogeneous distribution of LST obtained from the satellite images for the region was reduced. For many scientific studies and applications such as identifying geothermal resources, monitoring the trend of changes in the faults and volcanoes activities, the trend of thermal anomalies and their relationship with earthquake and management and planning of energy consumption in urban environment, the normalization of LST relative to environmental factors is of great importance. Future researches are warrant in this context to address the challenge of modeling relative humidity, air pressure, and wind speed for mountainous areas so as to improve the results of the surface energy balance modeling for LST normalization. Due to the complexity of urban areas, a limitation of the present research is the spatial resolution of thermal images. Improving spatial resolution of thermal images in future studies can increase the efficiency of the proposed model for modeling and normalizing LST in urban areas.

Acknowledgments

The authors would like to thank anonymous reviewers and the editor, Dr. Ashantha Goonetilleke, for providing constructive comments and suggestions which helped to improve the manuscript. We further acknowledge NASA/USGS for providing access to Landsat imagery. The authors also thank the International Relationship program, University of Tehran, for their great support in conducting this research.

Appendix A. Supplementary data

Supplementary data to this article can be found online at https://doi.org/10.1016/j.scitotenv.2018.09.027.

References

Anderson, M., Norman, J., Kustas, W., Houborg, R., Starks, P., Agam, N., 2008. A thermal-based remote sensing technique for routine mapping of land-surface carbon, water and energy fluxes from field to regional scales. Remote Sens. Environ. 112 (12), 4227–4241.
Bellaoui, M., Hassini, A., Bouchouicha, K., 2017. Remote sensed land surface temperature anomalies for earthquake prediction. Int. J. Eng. Res. Afr. 31, 120–134 (Trans Tech Publ.).
Benz, S.A., Bayer, P., Blum, P., 2017. Identifying anthropogenic anomalies in air, surface and groundwater temperatures in Germany. Sci. Total Environ. 584, 145–153.
Berger, C., Rosentreter, J., Voltersen, M., Baumgart, C., Schmullius, C., Hese, S., 2017. Spatio-temporal analysis of the relationship between 2D/3D urban site characteristics and land surface temperature. Remote Sens. Environ. 193, 225–243.
Bristow, K.L., 1987. On solving the surface energy balance equation for surface temperature. Agric. For. Meteorol. 39 (1), 49–54.
Chen, S.Y., Ma, J., Lliu, P.X., Liu, L.Q., 2009. A study on the normal annual variation field of land surface temperature in China. Chin. J. Geophys. 52 (5), 962–971.
Choudhury, B., Reginato, R., Idso, S., 1986. An analysis of infrared temperature observations over wheat and calculation of latent heat flux. Agric. For. Meteorol. 37 (1), 75–88.
Coolbaugh, M., Kratt, C., Fallacaro, A., Calvin, W., Taranik, J., 2007. Detection of geothermal anomalies using advanced spaceborne thermal emission and reflection radiometer (ASTER) thermal infrared images at Bradys Hot Springs, Nevada, USA. Remote Sens. Environ. 106 (3), 350–359.
Cooley, T., et al., 2002. FLAASH, a MODTRAN4-based atmospheric correction algorithm, its application and validation. Geoscience and Remote Sensing Symposium, 2002. IGARSS'02. 2002 IEEE International. vol. 3. IEEE, pp. 1414–1418.
Danielson, E.W., Levin, J., Abrams, E., 2003. Meteorology. McGraw-Hill.
de Paulo, J.M., Barros, J.E., Barbeira, P.J., 2016. A PLS regression model using flame spectroscopy emission for determination of octane numbers in gasoline. Fuel 176, 216–221.
Dozier, J., Outcalt, S.I., 1979. An approach toward energy balance simulation over rugged terrain. Geogr. Anal. 11 (1), 65–85.
Dubayah, R.C., 1994. Modeling a solar radiation topoclimatology for the Rio Grande River Basin. J. Veg. Sci. 5 (5), 627–640.
Eckmann, T.C., Roberts, D.A., Still, C.J., 2008. Using multiple endmember spectral mixture analysis to retrieve subpixel fire properties from MODIS. Remote Sens. Environ. 112 (10), 3773–3783.
Farifteh, J., Van der Meer, F., Atzberger, C., Carranza, E., 2007. Quantitative analysis of salt-affected soil reflectance spectra: a comparison of two adaptive methods (PLSR and ANN). Remote Sens. Environ. 110 (1), 59–78.
Fernández-Espinosa, A.J., 2016. Combining PLS regression with portable NIR spectroscopy to on-line monitor quality parameters in intact olives for determining optimal harvesting time. Talanta 148, 216–228.
Firozjaei, M.K., Kiavarz, M., Alavipanah, S.K., Lakes, T., Qureshi, S., 2018. Monitoring and forecasting heat island intensity through multi-temporal image analysis and cellular automata-Markov chain modelling: a case of Babol city, Iran. Ecol. Indic. 91, 155–170.
Friedl, M., 2002. Forward and inverse modeling of land surface energy balance using surface temperature measurements. Remote Sens. Environ. 79 (2), 344–354.
Glickman, T.S., Zenk, W., 2000. Glossary of Meteorology. American Meteorological Society.
Gutiérrez, F.J., Lemus, M., Parada, M.A., Benavente, O.M., Aguilera, F.A., 2012. Contribution of ground surface altitude difference to thermal anomaly detection using satellite images: application to volcanic/geothermal complexes in the Andes of Central Chile. J. Volcanol. Geotherm. Res. 237, 69–80.
Hantson, S., Chuvieco, E., 2011. Evaluation of different topographic correction methods for Landsat imagery. Int. J. Appl. Earth Obs. Geoinf. 13 (5), 691–700.
Harris, P.P., Folwell, S.S., Gallego-Elvira, B., Rodríguez, J., Milton, S., Taylor, C.M., 2017. An evaluation of modeled evaporation regimes in Europe using observed dry spell land surface temperature. J. Hydrometeorol. 18 (5), 1453–1470.
Jacobson, M.Z., 2005. Fundamentals of Atmospheric Modeling. Cambridge University Press.

Jain, S.K., Goswami, A., Saraf, A., 2008. Determination of land surface temperature and its lapse rate in the Satluj River basin using NOAA data. Int. J. Remote Sens. 29 (11), 3091–3103.
Jia, L., Marco, M., Bob, S., Lu, J., Massimo, M., 2017. Monitoring water resources and water use from Earth observation in the belt and road countries. Bull. Chin. Acad. Sci. 32 (Z1), 62–73.
Jiang, Y., Weng, Q., 2017. Estimation of hourly and daily evapotranspiration and soil moisture using downscaled LST over various urban surfaces. GISci. Remote Sens. 54 (1), 95–117.
Jiménez-Muñoz, J.C., Sobrino, J.A., Skoković, D., Mattar, C., Cristóbal, J., 2014. Land surface temperature retrieval methods from Landsat-8 thermal infrared sensor data. IEEE Geosci. Remote Sens. Lett. 11 (10), 1840–1843.
Kalogirou, S.A., 2013. Solar Energy Engineering: Processes and Systems. Academic Press.
Li, J., Song, C., Cao, L., Zhu, F., Meng, X., Wu, J., 2011. Impacts of landscape structure on surface urban heat islands: a case study of Shanghai, China. Remote Sens. Environ. 115 (12), 3249–3263.
Lievens, H., Martens, B., Verhoest, N., Hahn, S., Reichle, R., Miralles, D., 2017. Assimilation of global radar backscatter and radiometer brightness temperature observations to improve soil moisture and land evaporation estimates. Remote Sens. Environ. 189, 194–210.
Liu, Q., Liu, G., Huang, C., Liu, S., Zhao, J., 2014. A tasseled cap transformation for Landsat 8 OLI TOA reflectance images. Geoscience and Remote Sensing Symposium (IGARSS), 2014 IEEE International. IEEE, pp. 541–544.
Liu, Q., Liu, G., Huang, C., Xie, C., 2015. Comparison of tasselled cap transformations based on the selective bands of Landsat 8 OLI TOA reflectance images. Int. J. Remote Sens. 36 (2), 417–441.
Long, D., Singh, V.P., 2012. A two-source trapezoid model for evapotranspiration (TTME) from satellite imagery. Remote Sens. Environ. 121, 370–388.
Ma, J., Chen, S., Hu, X., Liu, P., Liu, L., 2010. Spatial-temporal variation of the land surface temperature field and present-day tectonic activity. Geosci. Front. 1 (1), 57–67.
Malbéteau, Y., et al., 2017. Normalizing land surface temperature data for elevation and illumination effects in mountainous areas: a case study using ASTER data over a steep-sided valley in Morocco. Remote Sens. Environ. 189, 25–39.
Mansor, S., Cracknell, A., Shilin, B., Gornyi, V., 1994. Monitoring of underground coal fires using thermal infrared data. Int. J. Remote Sens. 15 (8), 1675–1685.
Mattar, C., et al., 2014. Impacts of the broadband albedo on actual evapotranspiration estimated by S-SEBI model over an agricultural area. Remote Sens. Environ. 147, 23–42.
Merlin, O., Chehbouni, A., 2004. Different approaches in estimating heat flux using dual angle observations of radiative surface temperature. Int. J. Remote Sens. 25 (1), 275–289.
Merlin, O., Chehbouni, A.G., Kerr, Y.H., Njoku, E.G., Entekhabi, D., 2005. A combined modeling and multispectral/multiresolution remote sensing approach for disaggregation of surface soil moisture: application to SMOS configuration. IEEE Trans. Geosci. Remote Sens. 43 (9), 2036–2050.
Merlin, O., et al., 2010. Disaggregation of MODIS surface temperature over an agricultural area using a time series of Formosat-2 images. Remote Sens. Environ. 114 (11), 2500–2512.
Minder, J.R., Mote, P.W., Lundquist, J.D., 2010. Surface temperature lapse rates over complex terrain: Lessons from the Cascade Mountains. J. Geophys. Res. Atmos. 115 (D14).
Okalebo, J.A., et al., 2016. An evaluation of the community land model (version 3.5) and Noah land surface models for temperature and precipitation over Nebraska (Central Great Plains): implications for agriculture in simulations of future climate change and adaptation. Climate Change Adaptation, Resilience and Hazards. Springer, pp. 21–34.
Panah, S., Mogaddam, M.K., Firozjaei, M.K., 2017. Monitoring spatiotemporal changes of heat island in Babol city due to land use changes. Int. Arch. Photogramm. Remote. Sens. Spat. Inf. Sci. 42.
Peters, J., De Baets, B., De Clercq, E.M., Ducheyne, E., Verhoest, N.E., 2012. Influence of topographic normalization on the vegetation index–surface temperature relationship. J. Appl. Remote. Sens. 6 (1) (pp. 063518-1-063518-15).
Rapaport, T., Hochberg, U., Shoshany, M., Karnieli, A., Rachmilevitch, S., 2015. Combining leaf physiology, hyperspectral imaging and partial least squares-regression (PLS-R) for grapevine water status assessment. ISPRS J. Photogramm. Remote Sens. 109, 88–97.
Richter, R., Kellenberger, T., Kaufmann, H., 2009. Comparison of topographic correction methods. Remote Sens. 1 (3), 184–196.
Rigon, R., Bertoldi, G., Over, T.M., 2006. GEOtop: a distributed hydrological model with coupled water and energy budgets. J. Hydrometeorol. 7 (3), 371–388.
Rolland, C., 2003. Spatial and seasonal variations of air temperature lapse rates in Alpine regions. J. Clim. 16 (7), 1032–1046.
Silva, B.B.D., Braga, A.C., Braga, C.C., de Oliveira, L.M., Montenegro, S.M., Barbosa Junior, B., 2016. Procedures for calculation of the albedo with OLI-Landsat 8 images: application to the Brazilian semi-arid. Rev. Bras. Engenharia Agrícola Ambient. 20 (1), 3–8.
Sobrino, J.A., Jiménez-Muñoz, J.C., Paolini, L., 2004. Land surface temperature retrieval from LANDSAT TM 5. Remote Sens. Environ. 90 (4), 434–440.
Sobrino, J.A., et al., 2008. Land surface emissivity retrieval from different VNIR and TIR sensors. IEEE Trans. Geosci. Remote Sens. 46 (2), 316–327.
Stefan, V.G., Merlin, O., Er-Raki, S., Escorihuela, M.-J., Khabba, S., 2015. Consistency between in situ, model-derived and high-resolution-image-based soil temperature endmembers: towards a robust data-based model for multi-resolution monitoring of crop evapotranspiration. Remote Sens. 7 (8), 10444–10479.
Tucker, C.J., 1979. Red and photographic infrared linear combinations for monitoring vegetation. Remote Sens. Environ. 8 (2), 127–150.
Voogt, J.A., Oke, T.R., 2003. Thermal remote sensing of urban climates. Remote Sens. Environ. 86 (3), 370–384.
Walawender, J.P., Szymanowski, M., Hajto, M.J., Bokwa, A., 2014. Land surface temperature patterns in the urban agglomeration of Krakow (Poland) derived from Landsat-7/ETM+ data. Pure Appl. Geophys. 171 (6), 913–940.
Wan, Z., Wang, P., Li, X., 2004. Using MODIS land surface temperature and normalized difference vegetation index products for monitoring drought in the southern Great Plains, USA. Int. J. Remote Sens. 25 (1), 61–72.
Weng, Q., Lu, D., Schubring, J., 2004. Estimation of land surface temperature–vegetation abundance relationship for urban heat island studies. Remote Sens. Environ. 89 (4), 467–483.
Weng, Q., Hu, X., Quattrochi, D.A., Liu, H., 2014. Assessing intra-urban surface energy fluxes using remotely sensed ASTER imagery and routine meteorological data: a case study in Indianapolis, USA. IEEE J. Sel. Top. Appl. Earth Obs. Remote Sens. 7 (10), 4046–4057.
Wu, C., 2004. Normalized spectral mixture analysis for monitoring urban composition using ETM+ imagery. Remote Sens. Environ. 93 (4), 480–492.
Yu, X., Guo, X., Wu, Z., 2014. Land surface temperature retrieval from Landsat 8 TIRS—comparison between radiative transfer equation-based method, split window algorithm and single channel method. Remote Sens. 6 (10), 9829–9852.
Zheng, Y., Weng, Q., 2018. High spatial-and temporal-resolution anthropogenic heat discharge estimation in Los Angeles County, California. J. Environ. Manag. 206, 1274–1286.